frontiers | Frontiers in Materials

TYPE Original Research
PUBLISHED 30 May 2023
DOI 10.3389/fmats.2023.1180668

OPEN ACCESS

EDITED BY
Qichao Zhang,
Chinese Academy of Sciences (CAS), China

REVIEWED BY
Kaili Feng,
Tsinghua University, China
Jie Qiu,
Xi'an Jiaotong University, China

*CORRESPONDENCE
Yi Xu,
yixu@ncu.edu.cn

RECEIVED 06 March 2023
ACCEPTED 18 May 2023
PUBLISHED 30 May 2023

CITATION
Xia H, Xu Y, Duan J, Li S, Jiang N, Zhu S, Lei Y, Shi P and Tang J (2023), Tribological behaviors of Ta-10W alloy at elevated temperature.
Front. Mater. 10:1180668.
doi: 10.3389/fmats.2023.1180668

Tribological behaviors of Ta-10W alloy at elevated temperature

Haiqing Xia, Yi Xu*, Jing Duan, Shaoxuan Li, Nan Jiang, Shuai Zhu, Yaping Lei, Pengfei Shi and Jiancheng Tang

School ofPhysics and Materials Science, Nanchang University, Nanchang, China

Ta-10W alloy has great potential in the aerospace and nuclear industries due to its good formability, high melting point and excellent high-temperature strength. The purpose of this study was to experimentally research the tribological behaviors of Ta-10W at elevated temperatures and the effects of temperatures on the friction coefficient and the wear rate of Ta-10W in sliding wear. It was found that the main wear mechanism of the material at 100°C was abrasive wear, as well as adhesive wear and slight oxidative wear occurred at 200°C and 300°C. The friction coefficients increased as the temperature rose, which was attributed to the increase in metal viscosity at elevated temperatures. The wear rate gradually decreased with the temperature rising, such that there was a conversion from severe wear to light wear. At 200°C and 300°C, a large amount of stable oxide film covered the scar surface, resulting in decreased wear rate.

KEYWORDS

friction, Ta-10W, wear mechanism, oxides, elevated temperature (A)

1 Introduction

Ta-10W has great potential in the aerospace and nuclear industries due to its good formability, high melting point, excellent high-temperature strength and corrosion resistance (Byun and Maloy, 2008; Liu et al., 2018; Li et al., 2020; Lv et al., 2020). It has attracted considerable attention for high-temperature structural components in aerospace and the jacket for nuclear waste (Zhou et al., 2015; Novakowski et al., 2018; Wang et al., 2020; Zhang et al., 2020). Most of the workpiece surface failures are mainly caused by wear behaviors. Especially in some elevated-temperature areas, wear occurs frequently and inevitably. Therefore, it is necessary to research the wear mechanisms at elevated temperatures of Ta-10W alloy.

The tribological properties of Ta have been intensively investigated over the past decades. Kommel Lembit investigated the forming of gradient microstructures of pure tantalum under the wear trajectory of a dry sliding wear test (Kommel et al., 2021). The results showed that the coefficient of friction and wear was not dependent on the initial microstructure and hardness of the material, but the depth of the grading layer under the wear trajectory was dependent on the previous treatment history of the material. Many researchers had focused on the gradient nanocrystal structure consisting of recrystallized nanometer-sized grains formed under the surface layer of the sample when Ta was subjected to dry sliding friction (Zhang et al., 2014a; Zhang et al., 2014b). Notably, Ta has different phases, including metastable-tetragonal β-Ta and stable body-centered-cubic α-Ta phase. The β-Ta primarily has a high level of hardness, but it has a high level of brittleness and poor load-bearing ability. It is susceptible to fracture and wear under high load, which causes a high wear rate (Myers et al., 2013). Other studies showed the sample with tantalum gradient transitional layer showed excellent tribological properties, which were in close relation to the high critical load, low surface roughness and the phase transition from

TABLE 1 The element compositions of the Ta-10W plate materials (wt%).

W	Mo	Nb	Hf	C	O	Ta
8.7	-	-	-	-	-	91.3

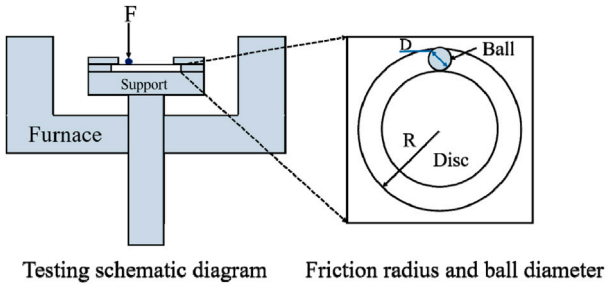

FIGURE 1
The sketch map of the high-temperature ball-on-disc friction and wear test setup.

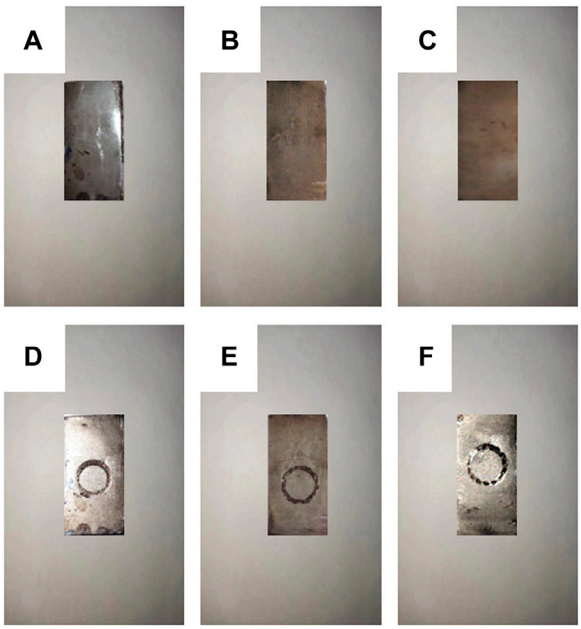

FIGURE 2
The macroscopic morphologies of specimens before and after wear at different temperatures of 4 N: before the wear: **(A)** 100°C, **(B)** 200°C, **(C)** 300°C; after the wear: **(D)** 100°C, **(E)** 200°C, **(F)** 300°C.

metastable β-Ta to stable cubic α-Ta under the action of frictional heat in oxygen-less conditions (Bing et al., 2022). Furthermore, tungsten has a uniform hardness, high melting point and superior oxidation resistance. The tungsten oxide formed in friction can protect the surface from damage (Li et al., 2017). Spark plasma sintering has been used in a few studies to consolidate Ta-W alloys. In a study by Shahram Seyyedin (Seyyedin et al., 2020), the effect of mechanical alloying time on the microstructure, hardness, and tensile properties of Ta-10 (wt%)W alloy sintered at 2000°C for 5 min using spark plasma sintering was investigated. Furthermore, the corrosion resistance of commercial purity titanium (CP-Ti) and Ti-6Al-4V (TC4) alloys coated with Ta-10W via multi-arc ion plating was investigated by Pei Sun, and electrochemical corrosion testing revealed that the Ta-10W coating improved the substrate's corrosion resistance (Sun et al., 2019). However, there isn't yet any research on the influence of temperature on the tribological properties of Ta-10W alloy.

In this study, the effect of temperature on the frictional properties of tantalum-tungsten alloys was examined. Like other superalloys, Ta-10W alloy would have a "pest" oxidation phenomenon at about 500°C (Dong et al., 2018), so the tribological tests at 100°C, 200°C and 300°C were carried out. Then, the elevated-temperature tribological samples were characterized by X-Ray diffractometer (XRD), Scanning Electron Microscopy (SEM) and Energy Dispersive Spectroscopy (EDS). The tribological behaviors and mechanisms of Ta-10W at elevated temperatures were studied.

2 Experimental

2.1 Materials

The Ta-10W plate provided by Ningxia Orient Tantalum Industry CO.LTD., which was made by electron beam melting, was used in this study. Samples with nominal dimensions of 20 mm × 10 mm × 1 mm were cut from the Ta-10W plate by electro-discharge machining for tribological tests. The element compositions of the Ta-10W plate materials were given in Table 1.

2.2 Wear tests

The elevated-temperature tribology tests were made with HT-1000 high-temperature tribology tester manufactured by Lanzhou Zhongke Kaihua Technology Development Co. LTD. The testing schematic diagram was given in Figure 1. The GCr15 bearing steel ball with a diameter of 5 mm was used as the friction pair and the radius of friction was 3 mm. The steel ball came with the instrument. The Vickers hardness was 800 HV and the accuracy was G10. The tests lasted for 30 min under the conditions of a constant load of 4 N and frequency of 10 Hz at elevated temperatures. The experiment temperature was raised to the required temperature by using the heating procedure (heating 10°C per minute), and the temperature was held for 30 min. After the test, we measured the mass difference of the sample before and after the tribology test with an analytical balance and calculated the wear rate (Shu et al., 2022) to investigate the wear resistance of the tested material. The wear rate was obtained from the following formula (Hu, 2010; Xu et al., 2018):

$$V = \frac{\Delta m}{\rho PS} \quad (1)$$

Where V is the wear rate of the sample in mm^3/Nm; Δm is the wear amount of the sample in mg; ρ is the sample density in g/cm^3; P is the load applied in the friction test in N; S is the sliding distance in m.

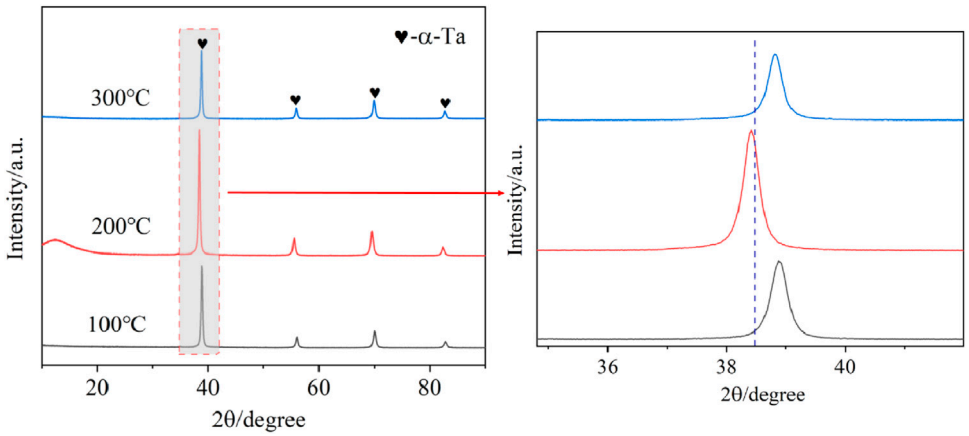

FIGURE 3
XRD patterns of the abrasion marks for different temperatures of 4 N.

2.3 Characterization methods

The morphology and microstructure of the wear marks on the surface of every sample were examined by SEM (Phenom LE, Phenom-Scientific, Shanghai, China, the accelerating voltage is 10 kV) and the elemental composition of the wear surface and friction film was studied by EDS analysis as part of the experimental work to characterize the wear mechanism of Ta-10W at elevated temperatures. Additionally, the worn surface was analyzed using XRD (Empyrean, PANalytical B.V., Netherlands).

3 Results

3.1 Wear surface analysis

Figure 2 gave the macroscopic morphologies of specimens before and after wear at different temperatures. It could be seen from the macroscopic morphology that the wear mark of 100°C was obviously larger than those of 200°C and 300°C. Figure 3 showed the XRD patterns of the abrasion marks for each temperature and those specially enlarged with the (110) pecks of every pattern. Diffraction peaks of (110), (200), (211), and (200) crystal planes were observed at the 38.5°, 55.5°,69.6°, and 82.4°, but no peaks of W appeared. In all curves, the tungsten peak had vanished, suggesting the dissolution of a large amount of available tungsten in the tantalum lattice (taking into account the quantitative comparison of the X-ray analysis and its errors) (Seyyedin et al., 2020), in the shape of the solid solution because of electron-beam smelting.

According to the Bragg equation:

$$2d \sin \theta = n\lambda \quad (2)$$

Where d is the distance between the crystal planes, θ is the incident ray, the angle between the reflection ray and the reflection crystal plane, λ is the wavelength, and n is the reflection series. The XRD diffraction peaks of (110) of materials for 100°C and 300°C experiments shifted to the right (the magnified peak referred to by the dotted line), indicating that the crystal plane spacing decreased, which was caused by lattice distortion in forging and rolling process when manufacturing the material.

The typical characteristics of the wear mark patterns on the Ta-10W surface after sliding tests at 100°C, 200°C, and 300°C were shown in Figures 4A, 5A, 6A, respectively. There were a lot of deep furrows in the wear marks at 100°C, and residual chips of different sizes (Figures 4B,C), which was a typical wear characteristic of abrasive wear. Abrasive wear is a very common and, at the same time, very serious type of wear. It arises when two interacting surfaces are in direct physical contact, and one of them is significantly harder than the other. Under the action of a normal load, the asperities on the harder surface penetrate the softer surface thus producing plastic deformations. When a tangential motion is introduced, the material is removed from the softer surface by the combined action of micro-ploughing and micro-cutting. And adhesive wear is invariably associated with the formation of adhesive junctions at the interface. When adhesive wear occurs, the material surface will always appear adhesive pull phenomenon (Stolarski, 1990). At 200°C, the wear of Ta-10W continued to reduce and there were no longer deep grooves to be found on the worn surface. The wear particles adhered to the wear surface and there was a successive tribolayer forming. An obvious accumulation of abrasive particles was found on both sides of the wear marks. Adhesion and drag phenomenon also appeared in the wear marks (Figure 5A). In addition, there were a few micro-cracks and spalling pits on the surface of the wear marks (Figures 5B,C). The main wear mechanism under this condition was adhesive wear. At 300°C, the wear surface was similar to that at 200°C, but the crack defects were more obvious and there were a few furrows (Figures 6B,C). EDS analyses of wear marks at all sliding test temperatures were performed. There was a C element on the surface of wear marks at 100°C and 200°C (Figures 7A,B), which was caused by the damage and peeling of steel balls during the wear process. Because of the detection of the O element, an oxide film including Ta and W (seen in Figures 7B, C) was formed at 200°C and 300°C.

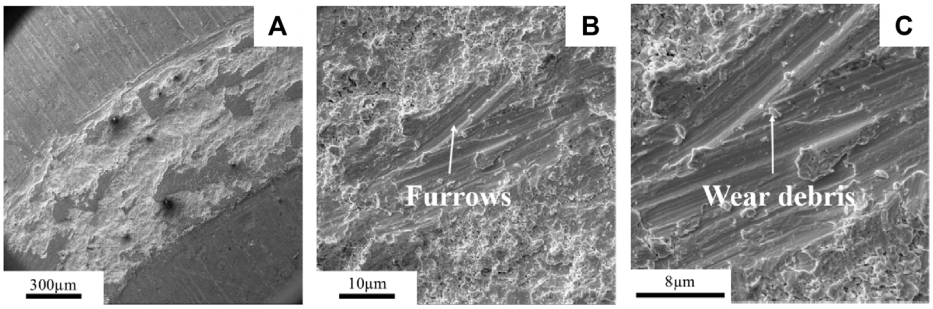

FIGURE 4
SEM micrographs of different multiples of the wear scar at 100°C of 4 N: **(A)** 180×, **(B)** 5000×, **(C)** 10000×.

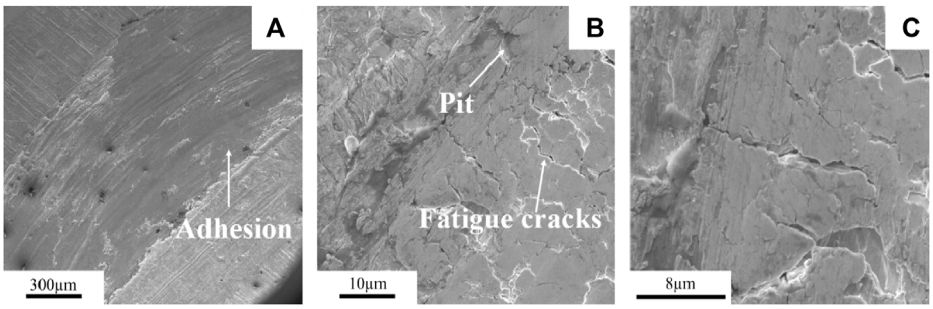

FIGURE 5
SEM micrographs of different multiples of the wear scar at 200°C of 4 N: **(A)** 180×, **(B)** 5000×, **(C)** 10000×.

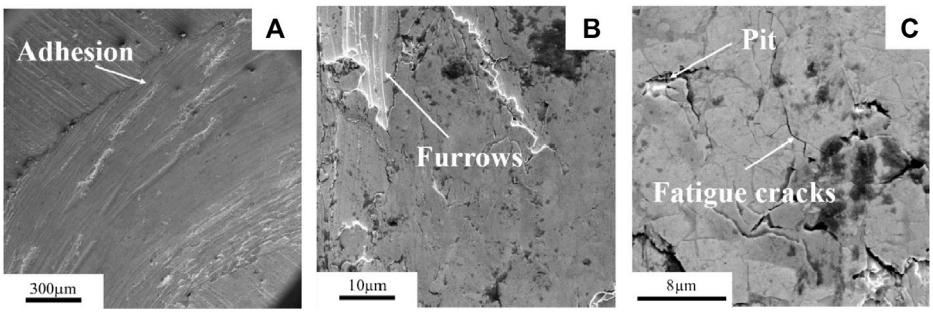

FIGURE 6
SEM micrographs of different multiples of the wear scar at 300°C of 4 N: **(A)** 180×, **(B)** 5000×, **(C)** 10000×.

3.2 Friction and wear

The friction coefficients and the wear rates were obtained from wear tests. Figure 8 showed the results of the friction coefficient for Ta-10W which were obtained at 100°C, 200°C, and 300°C. At the beginning of wear, it showed a rapidly rising trend, which was the run-in stage. The friction coefficient increased rapidly because the real area in contact between the grinding ball and the micro-bulge on the sample surface was small, the stress was large and the wear was intense (Xu et al., 2022). Then it entered the stable wear stage, and the average friction coefficients under the three conditions fluctuated close to the average level, with an average of 0.57, 0.58 and 0.66, which were obtained at 100°C, 200°C, and 300°C, respectively (Figure 8D). Cracks and spalling pits appeared on the wear scar surface at 200°C and 300°C (Figures 5B, 6C), which would aggravate the wear of the material surface, thus reducing the friction and wear performance of the material (Zhang et al., 2021). In addition, as the temperature rose, the viscosity of metal

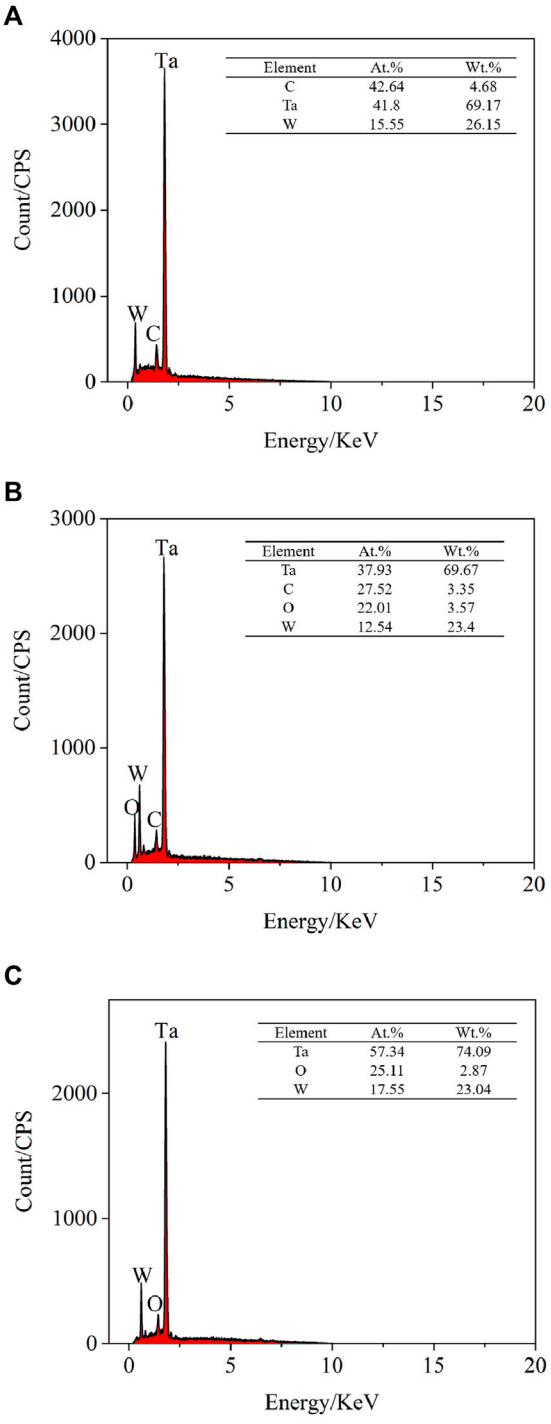

FIGURE 7
EDS micrographs of the wear scar at different temperatures of 4 N: **(A)** 100°C, **(B)** 200°C and **(C)** 300°C.

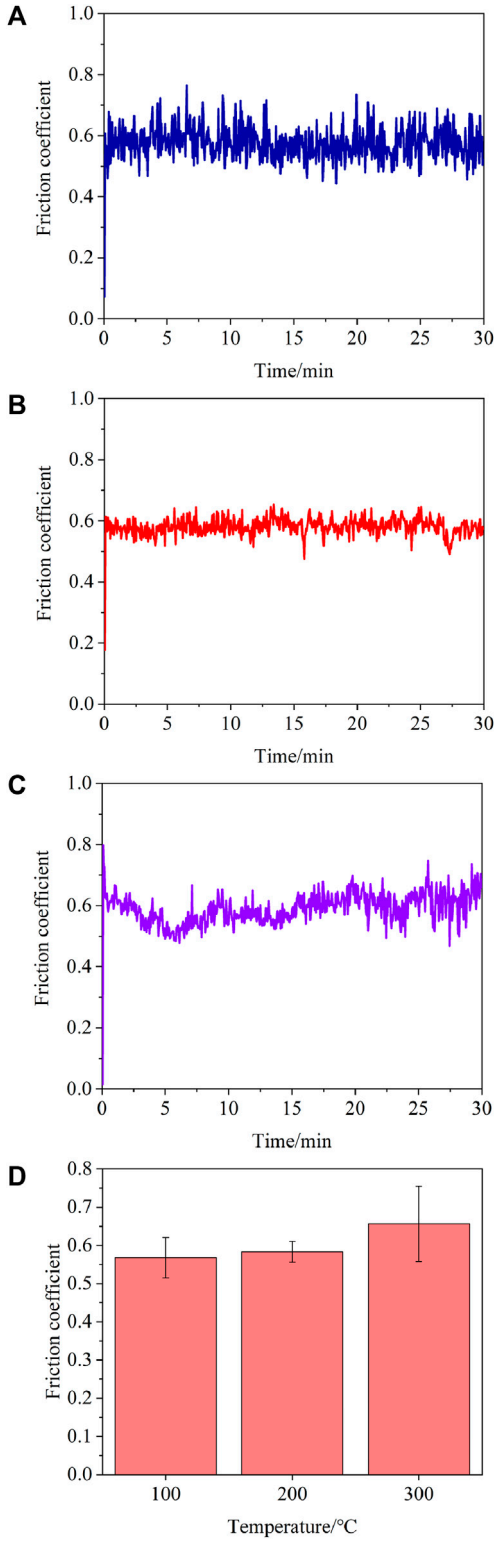

FIGURE 8
Friction coefficients of the Ta-10W with different temperatures of 4 N: **(A)** 100°C, **(B)** 200°C, **(C)** 300°C, and **(D)** average value.

increased, increasing the friction coefficient (Gautam et al., 2016). Therefore, as the temperature increased, the friction coefficient increased.

Figure 9 showed the typical 2-D surface contour measurement images of wear marks following the sliding wear tests between 100°C and 300°C. The areas surrounded by dashed lines and curves were the wear tracks. As shown in it, the wear track at 100°C had a maximum width of 942 μm. The widths of the wear tracks at 200°C and 300°C were 760 μm and 560 μm, respectively. Furthermore, as

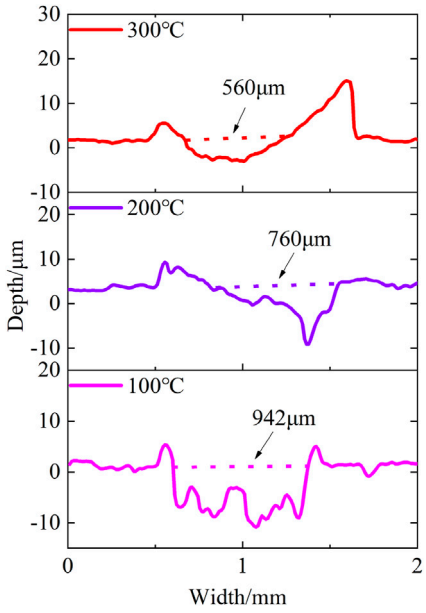

FIGURE 9
2-D surface contour measurement images of wear marks at different temperatures of 4 N.

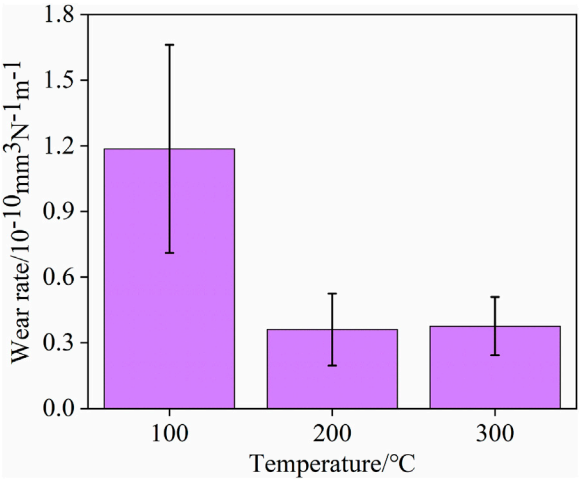

FIGURE 10
Wear rates of the Ta-10W with different temperatures of 4 N.

you could see from the figures that the volume of the wear track of 100°C was larger than 200°C and 300°C, which meant that the wear amount of 100°C was much more than 200°C and 300°C.

Figure 10 showed the wear rates of the Ta-10W with different temperatures. The average wear rates of Ta-10W for temperature condition of 100°C, 200°C, and 300°C at 4 N were 1.19×10^{-10} $mm^3N^{-1}m^{-1}$, 0.36×10^{-10} $mm^3N^{-1}m^{-1}$, and 0.38×10^{-10} $mm^3N^{-1}m^{-1}$, respectively. When the load was constant, the wear rate of Ta-10W tended to reduce with the increase in temperature. The weight loss revealed significant inflection points at 200°C (Table.2), and an abrupt decrease in the loss rate, indicating a change in the wear mechanism. As shown in 3.1, the main wear mechanism of the material changed from abrasive wear to adhesive wear, and there was slight oxidative wear at 200°C. Materials removed in elevated temperature tests were lower than the test of 100°C due to the formation of oxides at elevated temperatures. Partly oxidized alloy particles reduced the metal-metal contact and thus reduced the wear rate.

4 Discussions

It is well known that in the process of sliding contact when one surface moved over another surface, the movement of the surface would generate an interchangeable subsurface shear stress (Okonkwo et al., 2012). With the increase of wear time, the plastic strain of the subsurface layer gradually increased until cracks developed and extended to pits or spalling, as seen at 200°C and 300°C in this research. When the surface was lubed under these conditions, surface deformation was taken place, then the surface was elongated. Therefore, the surface showed a fish scale-like structure.

As Gautam G previously pointed out, the temperature rise may lead to the increase of material viscosity at high temperatures. It was reported that due to the temperature rose, the surface softening and excessive oxidation resulted in the continuous increase of friction coefficient (Gautam et al., 2016). Bai Yaping and Guo Yongchun also pointed out this phenomenon. They studied the influence of Al_2O_3 nanoparticles on the tribological behavior of 7,075 Al alloy and found that 7,075 Al alloy was easy to soften at high temperatures, which would lead to serious adhesion between 7,075 Al alloy and the corresponding vermicular cast iron. Thus, the friction coefficient raised with the increase in temperature (Bai et al., 2017).

The structure of tantalum oxide is complex and there are many phase structures, such as α phase, β phase, γ phase, and δ phase. Tantalum oxide films prepared by physical vapor deposition usually have an amorphous structure. When annealed in an air (or oxygen) atmosphere higher than the crystallization temperature (about 873–973 K), the crystal with an orthogonal crystal structure is mainly formed β-Ta_2O_5 (Dimitrova et al., 2001). In addition, Ta_2O_5 also has a body-centered cubic structure α-Ta_2O_5 and hexagonal crystal structure γ-Ta_2O_5. Tantalum oxide formed during friction did not show any features in the XRD pattern, which indicated that the atomic structure remained amorphous.

During the wear process, the scar surface was covered with a large number of stable oxide films, resulting in a reduction in the wear rate (Ahmadi et al., 2018). Figure 11 showed a schematic description of the friction film. In this work, the influence of oxide type and particle diameter on the transition behavior of light wear was studied (Kato and Komai, 2007). Wear had been reduced from severe wear to light wear. The transition to light wear was caused by the formation of wear protective film on the friction surface. It was observed that these friction films were generated by friction sintering of the provided oxide particles (Kato, 2008).

Particles are joined together during the sintering process by atomic transport events at temperatures below the melting point (German, 1984). Sintering is fueled by a decrease in the system's free energy, which is manifested as the elimination of surface area. Usually, sintering is controlled by atomic diffusion rates, which

TABLE 2 The average wear amounts and wear rates at different temperatures of 4 N.

Temperature/°C	Average wear amount/g	Average wear rate/10^{-10}mm^{3}N^{-1} m^{-1}
100	0.00253	1.19
200	0.00077	0.36
300	0.00080	0.38

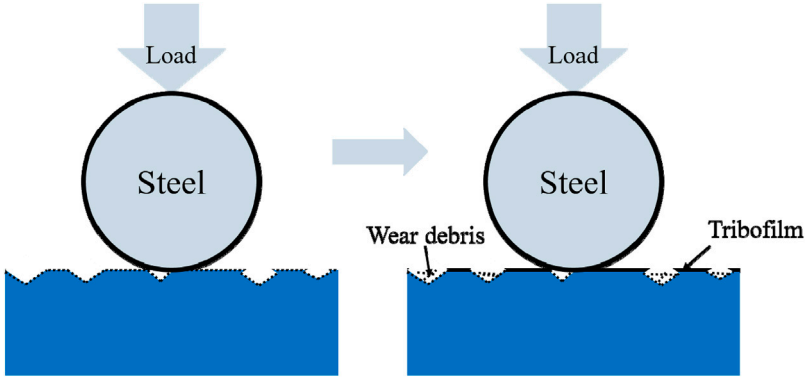

FIGURE 11
Schematic descriptions of tribofilms.

TABLE 3 Some oxides and their melting points.

Oxide type	Melting point/°C
CuO	1,446
Fe_2O_3	1,565
WO_2	1,473
Ta_2O_5	1800
TiO_2	1840
ZnO	1975
Al_2O_3	2054

are controlled by surfaces, grain boundaries, and lattices. Generally, the following formula may be used to express the sintering rate for particles, S:

$$S = a\frac{D^m}{d^n} \quad (3)$$

where D is the diffusion constant of part within the sintering material, d is the particle diameter, and a, m, and n are constants. Brown and Ashby (Brown and Ashby, 1980) had given the gas diffusion constant within the chemical compound, D as,

$$D = D_0 \exp\frac{QT_m}{RT} \quad (4)$$

Where D_0 is the diffusion frequency coefficient of about 5.3 × 10^{-4} m^2/s for oxides, Q is the activation energy of about 194.6 kJ/mol, R is the universal gas constant of about 8.3 J/mol K, T_m is the melting point of the oxide, and T is that the absolute temperature. This equation means that oxides at a low melting point or high temperature have relatively high diffusivity. Table 3 showed the melting points of some oxides. A study by Kato H showed that the provision of Fe_2O_3 and CuO nanoparticles caused a mild wear change under the conditions used, while the provision of Al_2O_3, ZnO or TiO_2 particles did not (Kato and Komai, 2007). Zhou et al. also reported that the addition of iron oxide particles during the friction process led to the formation of a friction layer (Zhou et al., 2018). Adachi Koshi proved the possibility of friction sintering of wear particles in the process of friction between alumina and itself under high operating pressure and high temperature through experiments (Adachi and Kato, 2000). The study of Zhou showed that for ultra-fine powder compacts, the sintering began as soon as the temperature increased from room temperature (Zhou et al., 1989). Several recent studies had indicated that the metal matrix properties could be augmented with particles such as Al_2O_3, Al_3Fe, or solid lubricants (graphite) (Yang et al., 2010; Agarwal et al., 2014; Li et al., 2015). When the tribological tests were carried out at 200°C and 300°C, tantalum oxide had a high diffusivity, thus forming a friction film, which changed the wear from heavy to light, so the wear rate decreased.

In addition, there were α-Ta nanoparticles assembled into nanoribbons on the reverse side, further reducing friction and wear (Bing et al., 2022). When the strength of the bonding point was lower than that of the two materials of the friction pair, shear occurred at the interface. At this point, the wear was very small, and the material transfer was not significant, although the friction coefficient increased. This slight

adhesive wear usually occurred when there was an oxide film, vulcanization film or another coating on the metal surface (Sun, 2007). So at 200°C and 300°C, the friction coefficients increased, but the wear rates were small.

5 Conclusion

The purpose of this study was to experimentally research the influence of temperature on the frictional wear of Ta-10W. Elevated-temperature tribological tests for Ta-10W with a normal load of 4 N and a time of 30 min were conducted. Using SEM and EDS, topography and morphology of the scars were performed.

The primary wear mechanism of the material at 100 °C was abrasive wear, and adhesive wear and slight oxidative wear occurred at 200°C and 300°C. The friction coefficients were graphed for different temperatures. The average friction coefficients under the three temperatures fluctuated close to the average level, with an average of 0.57, 0.58, and 0.66, respectively. It was observed that the friction coefficients increased with the temperature which was due to the increase of metal viscosity at elevated temperatures.

We measured the mass difference of the sample before and after the friction and wear test with an analytical balance and calculated the wear rates. The results indicated that the wear rate at 100°C was 1.19×10^{-10} $mm^3N^{-1}m^{-1}$, and the wear rates at 200°C and 300°C were greatly reduced, which were 0.36×10^{-10} $mm^3N^{-1}m^{-1}$ and 0.38×10^{-10} $mm^3N^{-1}m^{-1}$, respectively. It was observed that the wear rate decreased as the temperature increased, resulting in a transition from severe wear to light wear. At 200°C and 300°C, a large amount of stable oxide films covered the scar surface, resulting in a lower wear rate.

Data availability statement

The original contributions presented in the study are included in the article/supplementary material, further inquiries can be directed to the corresponding author.

Author contributions

HX and YX: conceptualization, methodology, experiment, data curation, writing. JD and SL: data curation, optimization. NJ and SZ: data curation, optimization. YL and PS: data curation, writing—review and editing. JT: conceptualization, methodology, supervision, project administration, writing and reviewing. All authors contributed to the article and approved the submitted version.

Acknowledgments

The authors gratefully acknowledge the financial support of the Natural Science Foundation, China (No. 51864034), Natural Science Foundation, Jiangxi Province, China (No. 20224BAB204016) and Jiangxi Province Graduate Innovation Special Fund Project (No. YC2022-S148).

Conflict of interest

The authors declare that the research was conducted in the absence of any commercial or financial relationships that could be construed as a potential conflict of interest.

The reviewer JQ is currently organizing a Research Topic with the author YX.

Publisher's note

References

Adachi, K., and Kato, K. (2000). Formation of smooth wear surfaces on alumina ceramics by embedding and tribo-sintering of fine wear particles. *Wear* 245 (1-2), 84–91. doi:10.1016/S0043-1648(00)00468-3

Agarwal, R., Mohan, A., Mohan, S., and Gautam, R. K. (2014). Synthesis and characterization of Al/Al3Fe nanocomposite for tribological applications. *J. Tribol.* 136 (1), 012001. doi:10.1115/1.4025601

Ahmadi, A., Sadeghi, F., and Shaffer, S. (2018). *In-situ* friction and fretting wear measurements of Inconel 617 at elevated temperatures. *Wear* 410, 110–118. doi:10.1016/j.wear.2018.06.007

Bai, Y., Guo, Y., Li, J., Yang, Z., and Tian, J. (2017). Effect of Al_2O_3 nanoparticle reinforcement on the mechanical and high-temperature tribological behavior of Al-7075 alloy. *Proc. Institution Mech. Eng. Part J J. Eng. Tribol.* 231 (7), 900–909. doi:10.1177/1350650116683627

Bing, Z., Liu, Y., Liu, Z., Ma, Y., Hei, H., Shi, B., et al. (2022). Improved tribological properties of stainless steel by high temperature-alloyed tantalum gradient layer. *Vacuum* 196, 110783. doi:10.1016/j.vacuum.2021.110783

Brown, A. M., and Ashby, M. F. (1980). Correlations for diffusion constants. *Acta Metall.* 28 (8), 1085–1101. doi:10.1016/0001-6160(80)90092-9

Byun, T. S., and Maloy, S. A. (2008). Dose dependence of mechanical properties in tantalum and tantalum alloys after low temperature irradiation. *J. Nucl. Mater.* 377 (1), 72–79. doi:10.1016/j.jnucmat.2008.02.034

Dimitrova, T., Arshak, K., and Atanassova, E. (2001). Crystallization effects in oxygen annealed Ta_2O_5 thin films on Si. *Thin Solid Films* 381 (1), 31–38. doi:10.1016/s0040-6090(00)01569-8

Dong, K., Zhao, G., Zhou, X., et al. (2018). The complex high temperature oxidation resistant coating for new type Ta10W alloy for aerospace purposes. *Yunnan Metall.* 47 (1), 50–56.

Gautam, G., Kumar, N., Mohan, A., Gautam, R. K., and Mohan, S. (2016). High-temperature tensile and tribological behavior of hybrid (ZrB2+ Al3Zr)/AA5052 *in situ* composite. *Metallurgical Mater. Trans. A* 47 (9), 4709–4720. doi:10.1007/s11661-016-3635-z

German, R. M. (1984). *Powder metallurgy science*. Princeton, New Jersey: Metal Powder Industries Federation.

Hu, X. (2010). *High temperature tribodogical properties and wear rate forecasting of molybdenum disilicide*. Wuhan, China: Wuhan University of Technology.

Kato, H. (2008). Effects of supply of fine oxide particles onto rubbing steel surfaces on severe–mild wear transition and oxide film formation. *Tribol. Int.* 41 (8), 735–742. doi:10.1016/j.triboint.2008.01.001

Kato, H., and Komai, K. (2007). Tribofilm formation and mild wear by tribo-sintering of nanometer-sized oxide particles on rubbing steel surfaces. *Wear* 262 (1-2), 36–41. doi:10.1016/j.wear.2006.03.046

Kommel, L., Podra, P., Mikli, V., and Omranpour, B. (2021). Gradient microstructure in tantalum formed under the wear track during dry sliding friction. *Wear* 466, 203573. doi:10.1016/j.wear.2020.203573

Li, G., Peng, N., Sun, D., and Sun, S. (2015). Friction and wear behavior of nano-Al_2O_3 particles reinforced copper matrix composites. *J. Tribol.* 137 (1), 011604. doi:10.1115/1.4028486

Li, J., Qin, L., Yang, K., Ma, Z., Wang, Y., Cheng, L., et al. (2020). Materials evolution of bone plates for internal fixation of bone fractures: A review. *J. Mater. Sci. Technol.* 36, 190–208. doi:10.1016/j.jmst.2019.07.024

Li, X., Yue, W., Wang, C., Liu, J., and Li, G. (2017). Preparation and structure of W/Mo films and their tribological properties in the lubrication of MoDTC. *J. Tribol.* 139 (6). doi:10.1115/1.4036175

Liu, Y., Liu, S., Deng, C., Fan, H., Yuan, X., and Liu, Q. (2018). Inhomogeneous deformation of {111}< uvw> grain in cold rolled tantalum. *J. Mater. Sci. Technol.* 34 (11), 2178–2182. doi:10.1016/j.jmst.2018.03.015

Lv, Y., Hu, K., Huang, Z., Cao, Z., Wen, S., Zhao, Y., et al. (2020). Effect of tungsten on the vacancy behaviors in Ta–W alloys from first-principles calculations. *Solid State Commun.* 306, 113767. doi:10.1016/j.ssc.2019.113767

Myers, S., Lin, J., Souza, R. M., Sproul, W. D., and Moore, J. J. (2013). The β to α phase transition of tantalum coatings deposited by modulated pulsed power magnetron sputtering. *Surf. Coatings Technol.* 214, 38–45. doi:10.1016/j.surfcoat.2012.10.061

Novakowski, T., Sundaram, A., Tripathi, J., Gonderman, S., and Hassanein, A. (2018). Deuterium desorption from ion-irradiated tantalum and effects on surface morphology. *J. Nucl. Mater.* 504, 1–7. doi:10.1016/j.jnucmat.2018.03.023

Okonkwo, P. C., Kelly, G., Rolfe, B. F., and Pereira, M. P. (2012). The effect of temperature on sliding wear of steel-tool steel pairs. *Wear* 282, 22–30. doi:10.1016/j.wear.2012.01.017

Seyyedin, S., Zangi, H., Bozorgmehr, M., Ghasemi, B., Tavallaei, M. M., and Adib, S. (2020). The effect of mechanical alloying time on the microstructural and mechanical properties of spark plasma sintered Ta–10W. *Mater. Sci. Eng. A* 798, 140024. doi:10.1016/j.msea.2020.140024

Shu, K., Wang, W., Ding, H., Lin, Q., Meli, E., Guo, J., et al. (2022). Influence of sand transport rate on rolling wear and damage behaviors of wheel/rail in Gobi and desert windblown sand environments. *Tribol. Int.* 172, 107584. doi:10.1016/j.triboint.2022.107584

Stolarski, T. (1990). *Tribology in machine design*. South Norwalk, Connecticut: Industrial Press Inc.

Sun, J. (2007). *Material forming wear and lubrication*. Arlington, Virginia: Nation Defense Industry Press.

Sun, P., Gu, Y., Li, Y., and Liu, B. (2019). Corrosion behavior of Ta-10W coatings on CP-Ti and TC4 substrates. *J. Mater. Eng. Perform.* 28, 4152–4162. doi:10.1007/s11665-019-04175-z

Wang, S., Wu, Z., Xie, M., Si, D., Chen, C., et al. (2020). The effect of tungsten content on the rolling texture and microstructure of Ta-W alloys. *Mater. Charact.* 159, 110067. doi:10.1016/j.matchar.2019.110067

Xu, J., Tan, W., Hu, Z., Wang, S., and Zhou, J. (2022). High temperature friction and wear properties of laser surface texturing of TC4 titanium alloy. *Laser & Optoelectron. Prog.* 59 (11), 1114002. doi:10.3788/lop202259.1114002

Xu, Y., Liang, W., Miao, Q., Wang, L., Ren, B., Cui, S.-Y., et al. (2018). Enhanced high temperature corrosion resistance of Al_2O_3/Al composite coating on γ -TiAl alloy. *Rare Metal Mater. Eng.* 47 (4), 1075–1081. doi:10.1016/s1875-5372(18)30123-1

Yang, Y., Jia, Z., Chen, J., et al. (2010). *Tribological behaviors of PTFE-based composites filled with nanoscale lamellar structure expanded graphite*.

Zhang, H., Li, D., and Liang, Z. (2021). Novel endoscopic optical diagnostic technologies in medical trial research: Recent advancements and future prospects. *J. Shenyang Ligong Univ.* 40 (2), 5. doi:10.1186/s12938-020-00845-5

Zhang, T., Deng, H., Xie, Z., Liu, R., Yang, J., Liu, C., et al. (2020). Recent progresses on designing and manufacturing of bulk refractory alloys with high performances based on controlling interfaces. *J. Mater. Sci. Technol.* 52, 29–62. doi:10.1016/j.jmst.2020.02.046

Zhang, Y., Wei, Q., Niu, H., Chen, C., Yu, Z., et al. (2014). Formation of nanocrystalline structure in tantalum by sliding friction treatment. *Int. J. Refract. Metals Hard Mater.* 45, 71–75. doi:10.1016/j.ijrmhm.2014.03.011

Zhang, Y., Zhang, P., Niu, H., Chen, C., Wang, G., Xiao, D., et al. (2014). Surface nanocrystallization of Cu and Ta by sliding friction. *Mater. Sci. Eng. A* 607, 351–355. doi:10.1016/j.msea.2014.03.089

Zhou, L., Zhang, Q., Zeng, X., Danzheng, J., Zheng, Q., Liu, J., et al. (2015). Transcriptional and proteomic analyses of two-component response regulators in multidrug-resistant *Mycobacterium tuberculosis*. *J. Of Wuhan Univ. Of Technol.* 37 (12), 73–81. doi:10.1016/j.ijantimicag.2015.02.018

Zhou, Y. H., Harmelin, M., and Bigot, J. (1989). Sintering behaviour of ultra-fine Fe, Ni and Fe-25wt%Ni powders. *Scr. Metall.* 23, 1391–1396. doi:10.1016/0036-9748(89)90065-3

Zhou, Y., Jiang, W., Chen, W., Ji, X. L., Jin, Y. X., and Wang, S. Q. (2018). Modification of tribolayers of a titanium alloy sliding against a steel. *J. Tribol.* 140 (4), 042301. doi:10.1115/1.4039162